


Attosecond Dynamics of *sp*-Band Photoexcitation

Johann Riemensberger^{1,2,*}, Stefan Neppel^{1,†}, Dionysios Potamianos^{1,2}, Martin Schäffer¹, Maximilian Schnitzenbaumer¹,
 Marcus Ossiander^{1,2}, Christian Schröder¹, Alexander Guggenmos^{2,3,‡}, Ulf Kleineberg^{2,3}, Dietrich Menzel¹,
 Francesco Allegretti¹, Johannes V. Barth¹, Reinhard Kienberger¹, and Peter Feulner¹
¹*Physik Department, Technische Universität München, James-Frank-Str 1, 85748 Garching, Germany*
²*Max-Planck Institut für Quantenoptik, Hans-Kopfermann-Str. 1, 85748 Garching, Germany*
³*Fakultät für Physik, Ludwig-Maximilians-Universität München, Am Coulombwall 1, 85748 Garching, Germany*

Andrei G. Borisov^{4,5}, Pedro M. Echenique⁵, and Andrey K. Kazansky^{5,6}
⁴*Institut des Sciences Moléculaires d'Orsay (ISMO), UMR 8214, CNRS, Université Paris Sud,
 Université Paris-Saclay, bât 520, F-91405 Orsay, France*
⁵*Material Physics Center CSIC-UPV/EHU; Donostia International Physics Center DIPC,
 Paseo Manuel de Lardizabal 5 20018, Donostia-San Sebastián, Spain*
⁶*IKERBASQUE, Basque Foundation for Science, 48013 Bilbao, Spain*

 (Received 26 February 2019; revised manuscript received 3 June 2019; published 21 October 2019)

We report measurements of the temporal dynamics of the valence band photoemission from the magnesium (0001) surface across the resonance of the $\bar{\Gamma}$ surface state at 134 eV and link them to observations of high-resolution synchrotron photoemission and numerical calculations of the time-dependent Schrödinger equation using an effective single-electron model potential. We observe a decrease in the time delay between photoemission from delocalized valence states and the localized core orbitals on resonance. Our approach to rigorously link excitation energy-resolved conventional steady-state photoemission with attosecond streaking spectroscopy reveals the connection between energy-space properties of bound electronic states and the temporal dynamics of the fundamental electronic excitations underlying the photoelectric effect.

DOI: [10.1103/PhysRevLett.123.176801](https://doi.org/10.1103/PhysRevLett.123.176801)

Photoemission is the standard method for the investigation of occupied electronic states, for isolated atoms and molecules and in condensed matter systems, including samples of demanding complexity [1]. The timing of the photoemission process, i.e., the time elapsing between photon absorption and electron emission, is experimentally accessible since laser sources producing synchronized attosecond extreme-ultraviolet (XUV) pump pulses and few-cycle near-infrared (NIR) waveforms are available [2] and its investigation considerably enhances our understanding of fundamental light-matter interactions [3,4]. Experiments yield relative delays between photoelectrons from different initial states, which by comparison with appropriate reference states and theory can be turned into absolute values with high precision [5]. For isolated particles, particularly light atoms, this time interval, which is commonly denoted as (absolute) delay can be calculated with attosecond precision [6,7]. Yet, for condensed matter systems, theoretical investigations are much more demanding and mostly limited to 1D model systems [8–11] or semiclassical treatment [12,13]. Furthermore, suitable high-precision references cannot always be obtained easily and ambiguities may remain. To this end, we introduce a holistic study of the dynamical photoemission process by rigorously combining time- and energy-resolved

attosecond streaking spectroscopy with conventional high-resolution spectroscopy and numerical calculations based on the solution of the time-dependent Schrödinger equation (TDSE) over a broad excitation region spanning from the XUV into the soft-x-ray (SXR) region.

Of particular interest is the identification and dissection of the measured photoemission time delay into the constituting microscopic origins of the observed retardation. For prototypical solid materials XUV penetrates deeply, whereas the NIR radiation is reflected or refracted at the surface [14,15]. Thus the probing of the photoelectrons starts as they traverse the substrate-vacuum boundary and not at their sites of generation. Photoemission delay due to electron transport inside the material dominates at larger kinetic energy, when atomic delays are shown to become small [6,16]. Inelastic and elastic scattering limit the escape depth to the outermost atomic layers [13]. In general, resonant photoemission, which involves transitions between bulk bands, allows larger escape depth and therefore larger delays than nonresonant photoemission with transitions into waves that do not propagate in the bulk. This has been predicted theoretically in Ref. [10] and demonstrated experimentally by Tao *et al.* [17], who furthermore report a correlation between the delay values obtained by attosecond pump-probe experiments and by

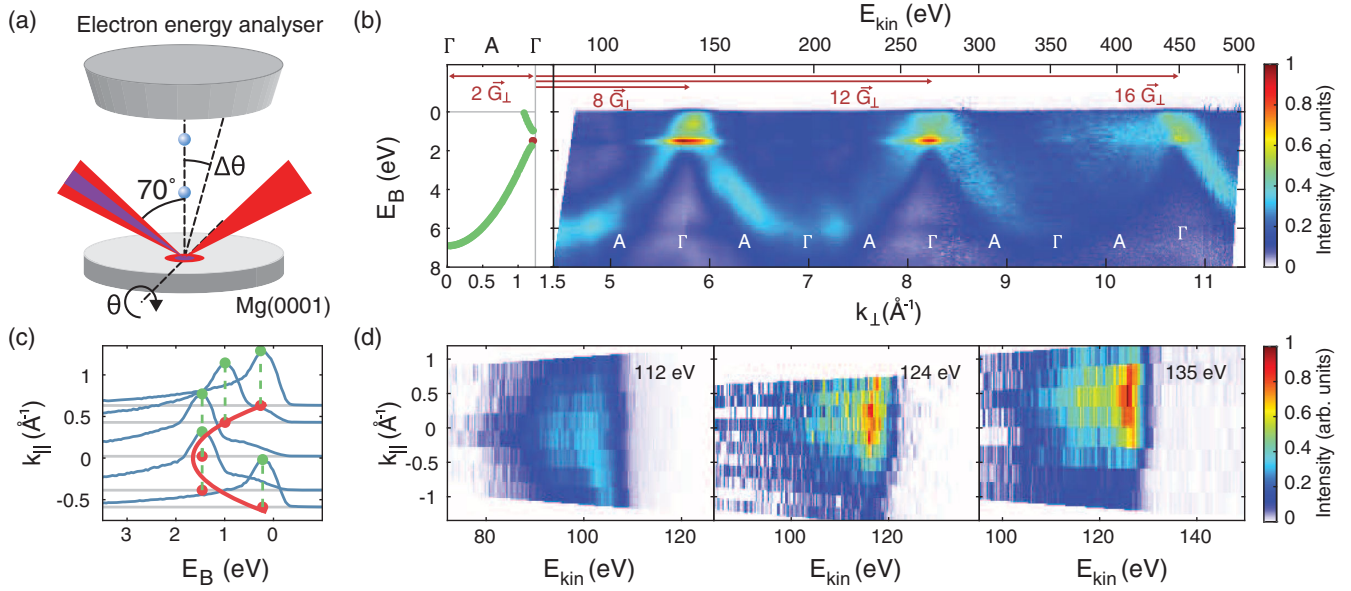


FIG. 1. (a) Experimental geometry of attosecond and synchrotron photoemission experiments. XUV radiation and NIR radiation (time-resolved experiment only) are focused on a Mg(0001) surface. The emission angle θ is varied by tilting the sample (laser experiment) or rotation of the detector (synchrotron); the angular resolution $\Delta\theta$ is determined by the electron energy analyser. (b) (Left) Occupied part of Mg(0001) band structure perpendicular to the surface. The surface state lies at the lower edge of the band gap and is indicated in dark red. (Right) Experimental photoemission spectrogram recorded with narrow band synchrotron radiation in normal emission geometry. The resonant photoemission bands arise from direct bulk transitions conserving the band momentum in the reduced zone scheme. Red arrows mark the resonant photoemission of the surface state in the extended zone scheme. (c) ARPES at 130 eV photon energy displaying the parabolic dispersion of the Shockley-type $\bar{\Gamma}$ surface state. (d) ARPES recorded with isolated attosecond pulses. See main text for details.

applying the $[\Delta E, \Delta t]$ uncertainty relation to the spectral width of the resonance, therefore enabling delay estimates also from static photoemission data [18]. However, recent studies of the link between photoelectron retardation and the material band structure focused entirely on the properties of the final states [17,19,20] at photon energies below 30 eV.

As yet, to the best of our knowledge, no study comparing energy-, angle- and time-resolution and covering resonant and nonresonant photoemission from surface and bulk valence states and from inner-shell states has been performed. This applies especially to the high-energy XUV and SXR spectral regions, where delays are generally small (<100 as) and necessitate highly precise measurements. Here, we close this gap by comparing attosecond streaking and static photoemission data from the Mg(0001) surface at, below, and above the 2nd resonance of its $\bar{\Gamma}$ Shockley-type surface state at 134 eV excitation energy. Our study covers most of the band structure induced effects, especially those related to the initial state, and elucidates the opposing actions of surface localization, e.g., of a surface state compared to bulk bands, and the extended electron escape depth on resonance. Further comparison to numerical solutions of the 1D TDSE based on an established model potential reveals how the specific structures of the initial valence state wave functions influence the observed attosecond retardation of the photoelectric effect.

The experimental geometry of the presented photoemission experiments is depicted in Fig. 1(a). *p*-polarized XUV and SXR radiation impinges on the surface at 70° for attosecond ($110 \text{ eV} < \hbar\omega < 145 \text{ eV}$) and 83° for synchrotron experiments ($90 \text{ eV} < \hbar\omega < 500 \text{ eV}$), with respect to the surface normal. In order to establish a correlation between steady-state and attosecond photoemission spectroscopies, we performed photon energy-dependent measurements with narrow-band synchrotron radiation at the U49/2-PGM1 beam line at the Helmholtz-Zentrum Berlin. The results are plotted in Fig. 1(b) and reveal a photoemission spectrogram dominated by the periodic bands of resonant photoemission overlapping at the surface state resonances at 134, 262, and 450 eV. These features are observed due to direct transitions between the occupied and unoccupied dominant free electronlike band in Mg [21] and similar observations have been made for *sp*-band photoemission in Cu(111) and Al(100) [22,23] deep into the SXR spectral region. The occupied portion of the Mg(0001) band structure, calculated with the 1D quantum mechanical model, is depicted in the left panel of Fig. 1(b). The projection onto the surface normal effectively halves the size of the hcp unit cell, hence the crystal momentum exchanged in the direct transitions is doubled. The in-plane dispersion of the bulk and surface states, measured with angle-resolved photoemission spectroscopy [ARPES, see Fig. 1(c)] at 130 eV, yields effective masses close to

unity $m^*/m_e = 1.1 \pm 0.2$, in agreement with earlier results [21,24].

A detailed account of the attosecond photoemission spectroscopy apparatus has been published elsewhere [25]. Isolated attosecond pulses are obtained from high-harmonic generation with the amplitude gating scheme in the cutoff region and spectral filtering using thin Zr and Pd films as well as four custom multilayer reflectors [26]. ARPES with isolated attosecond pulses is performed in order to confirm the existence of the photoemission resonance for illumination with broadband isolated attosecond pulses. The results are depicted in Fig. 1(d). Each valence band spectrum is divided by the photocurrent of the Mg 2*p* core level after background subtraction [27] at the same photon energy and emission angle. Approaching the photoemission resonance, two effects in the ARPES spectra are observed. First, the photoemission intensity is shifted progressively towards the Fermi edge in accordance with the results from high-resolution synchrotron photoemission spectroscopy [see Figs. 1(b), 1(d)]. Second, we observe strong enhancement of the photocurrent from the delocalized valence band around the Γ -point despite the poor spectral resolution associated with isolated attosecond pulses. This enhancement results from the parabolic dispersion of the $\bar{\Gamma}$ -surface state [21,24], which appears below the Fermi edge of Mg(0001) only for in-plane momenta $k_{\parallel} < 0.67 \text{ \AA}^{-1}$ and is consistent with our own ARPES results at 130 eV photon energy [see Fig. 1(c)].

We measure the relative time-delay $\Delta\tau$ between the photoemission from the Mg(0001) valence band (VB) and Mg 2*p* core level under variation of the photon energy to probe the retardation effect of the photoemission resonance. A positive value of $\Delta\tau$ indicates VB electrons leaving the crystal first. Figure 2(a) illustrates the attosecond streaking experiment along with the static broadband photoemission spectrum. Spectrograms are recorded by focusing both the XUV and NIR laser pulses onto the Mg(0001) surface. The angle of acceptance of the time-of-flight (TOF) spectrometer for electrons is $\pm 2^\circ$ around the surface normal; it can be increased to $\pm 22^\circ$ with an electrostatic Einzel lens. The experimental delay retrieval schemes are modeled after Refs. [4,28] and detailed in the Supplemental Material [29]. A pronounced minimum of $\Delta\tau$ of Mg 2*p* photoemission is observed coinciding with the resonance of the surface state for both narrow- and wide-angle photoemission. At photon energies of 124 and 135 eV, $\Delta\tau$ is almost vanishing (≈ 12 as). Exciting with photons below and above this energy window, we observe 40 as as an increase of $\Delta\tau$, i.e., advancement of the VB photoemission. We note that the increase of $\Delta\tau$ is only slightly smaller if we integrate over several full Brillouin zones ($\pm 22^\circ$).

Theoretically, the dynamics of one-electron photoemission from solids in attosecond streaking can be described by solving the TDSE in the single-active electron approximation. This approach provides a full three-step treatment

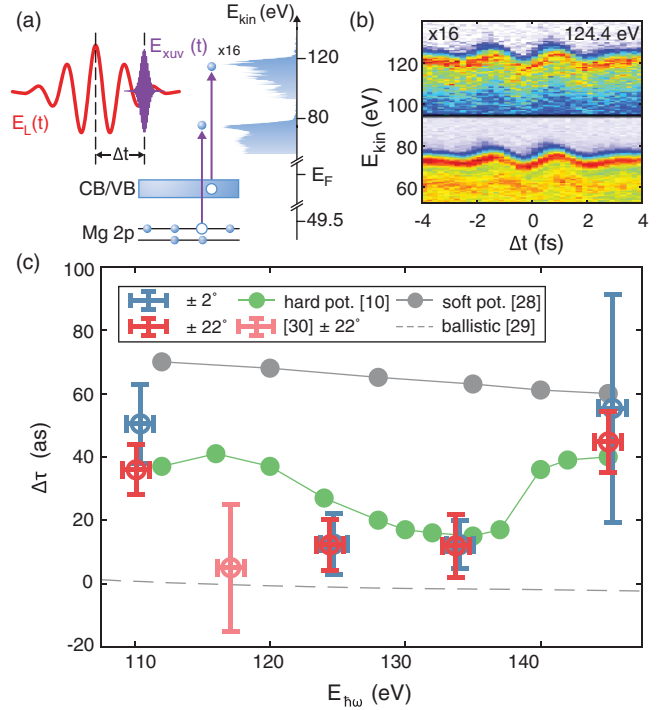


FIG. 2. (a) Schematic of the attosecond streaking spectroscopy. XUV (purple) and IR (red) pulses with controlled time delay Δt are focused on the Mg(0001) surface and expel electrons (blue) from the Mg 2*p* states and valence band (VB) levels. The steady-state photoelectron spectrum, recorded at 124.4 eV photon energy, is indicated in blue on the right. (b) Attosecond streaking spectrogram recorded at 124.4 eV. (c) Energy-dependent relative attosecond time delays $\Delta\tau$ of the Mg 2*p* core level for small ($\pm 2^\circ$, blue) and large ($\pm 22^\circ$, red) electron detection regions and relative time delays obtained from numerical calculations with the effective single-electron model potentials (hard potential [10] (green), soft potential [37] (gray)). Classical transport theory predicts nearly vanishing time delays for purely ballistic electron propagation [14,38] (gray, dashed). The light red point represents the result from Ref. [28].

of photoemission, wherein the XUV photon absorption, electron propagation in the solid, and its motion in vacuum under action of the IR field are treated on equal footing. While a complete 3D numerical calculation is presently out of reach, the computational problem can be greatly simplified considering the experimental geometry with attosecond streaking spectrograms recorded for electron emission along the surface normal and with *p*-polarized IR and XUV pulses. This approach, addressing only the electronic structure of the substrate perpendicular to the surface, has been already successfully implemented to explain photoemission time delays of van der Waals crystals [16]. We solved the TDSE for the 1D model potential representation of Mg(0001) [10] depicted in Fig. 3(a). The model potential is constructed starting from the model potential established by Chulkov *et al.* for Mg(0001) [37] and adding a Gaussian-type repulsive core

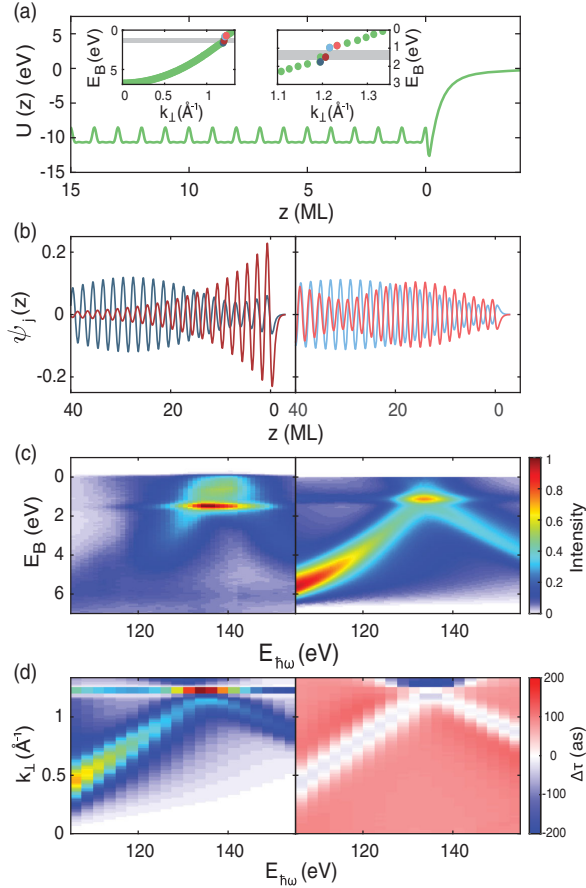


FIG. 3. (a) Effective single-electron potential $U(z)$ (green) of the electron-metal interaction as a function of distance from the metal surface in units of the Mg(0001) interlayer spacing (in monolayers, ML). Inset: Band structure of occupied states for a 68 layer Mg(0001) slab. States marked in blue and red are plotted in Fig. 3(b). Gray shaded area marks the projected band gap. (b) Wave functions of occupied states around the $\bar{\Gamma}$ -band gap. The symmetric surface state is plotted in dark red. The wave function of the state with highest energy below the gap is plotted in dark blue. The first and second states above the projected band gap are plotted in light colors. (c) Comparison of experimental (left) and simulated (right) photoemission spectrograms in normal emission geometry around the 2nd resonance of the $\bar{\Gamma}$ surface state, taking into account the finite collection angle of the analyzer. (d) (Left) Normalized partial intensity of calculated photocurrent emitted from each individual bound state k_{\perp} [color scale same as Fig. 3(c)]. The strong emission at $k_{\perp} = 1.21 \text{ \AA}^{-1}$ marks the $\bar{\Gamma}$ surface state in the projected band gap. (Right) Relative time delay of Mg $2p$ photoemission with respect to individual bound states. Positive values indicate the VB electrons leaving the crystal first.

potential at each atomic position, which represents the interactions between valence and core electrons in Mg [10]. The 1D TDSE is solved in the rotating wave approximation (RWA) separately for each initial state characterized by the momentum perpendicular to the surface k_{\perp} and an energy $E_{k_{\perp}}$ within the occupied portion of the VB. Full spectrograms are obtained by incoherent summation.

Further details of the numerical model are found in Ref. [8] and the Supplemental Material [29].

In Fig. 3(c), we compare the experimental high-resolution photoemission spectrogram with the numerical result accounting for the finite angular detection region of the electron analyzer (see Supplemental Material [29]). Our numerical calculation reproduces both the position and bandwidth of the resonant photoemission bands as well as the $\bar{\Gamma}$ surface state resonance. The high-resolution photoemission spectrograms are well understood within the framework of 1-step photoemission theory [39], which, however, does not provide any information of the underlying temporal dynamics of photoexcitation. In Fig. 2(c), we furthermore compare classical and quantum mechanical calculations with the experimental results for the attosecond electron dynamics. Classical transport theory, based on measured mean escape depths, predicts vanishing relative time delays [14,28], which roughly agrees with the experimental results between 117 and 134 eV, but disagrees farther away from the surface state resonance. However, we find broad agreement between experiment and the full quantum-mechanical theory. Especially the observed nonmonotonic dependency of $\Delta\tau$ between 124 and 145 eV, i.e., resonant photoemission close to the Brillouin zone boundary, is reproduced in the numerical calculation. Similar calculations employing the original potential proposed by Chulkov *et al.* [37], which lacks the higher order spatial harmonics introduced with the repulsive core potential, predict purely nonresonant photoemission and a nearly constant relative time delay around 65 as [10]. We find the calculated absolute Mg $2p$ time delay (≈ 80 as) to be weakly dependent on the photon energy, in agreement with classical transport theory. Hence, we attribute the observed effect to increasing VB retardation around 130 eV, despite the enhanced photoemission from the $\bar{\Gamma}$ -surface state [10]. We tentatively ascribe the discrepancy between the earlier experimental result at 117 eV [see Fig. 2(c), (light red) and Ref. [28]] and the present calculations to the limitations of the 1D quantum mechanical model used here for the generally speaking 3D problem of the photoemission from the Mg(0001) surface. This assignment is motivated by the experimental observation of a local minimum of the resonant bulk photoemission intensity at excitation energies between 110 and 120 eV [see Figs. 1(b) and 3(c)], which is not reproduced by the numerical computations.

Within the quantum theory, the photoemission is determined by the contributions from the bulk and surface regions. The former corresponds to the interband transitions between the occupied and empty states characterized by the same electron momentum, and the electrons are emitted from the depth determined by their inelastic mean free path. The anomaly arises when the resonant transition from the initial valence state to the final conduction band state occurs at the vicinity of the Brillouin zone boundary

$2G_{\perp} = 1.21 \text{ \AA}^{-1}$. Figure 3(d) depicts the partial photocurrent emerging from the individual initial states k_{\perp} as a function of photon energy and their relative time delays with respect to the Mg $2p$ states. Two aspects dominate the temporal dynamics around the surface state resonance: First, the surface state itself, contrary to the case of tungsten [5], protrudes significantly into the crystal bulk and on resonance its photoemission delay rises by 80 as compared with the off-resonant case. Hence, we conclude that Shockley-type surface states, especially if located close to the band edge, in contrast to image-charge [12] or adsorbate states [5,38], do not pose well-defined reference markers for the absolute timing of photoemission events.

More importantly, because of the orthogonality constraint with respect to the surface state and considering the structure of the Bloch waves at the Brillouin zone boundary, the wave function of the bound states, which are located above the projected band gap $k_{\perp} > 2G_{\perp}$, $E_B < 1.5 \text{ eV}$, are repelled from the surface into the metal bulk [see Fig. 3(b), right panel]. This implies a shift of the region of resonant XUV absorption into the solid, strongly delaying their photoemission response by more than 150 as, which is confirmed by performing initial-state resolved time delay analysis of the numerical photoemission spectra, depicted in the right panel of Fig. 3(d). The resonant enhancement of the above-gap states is asymmetric around the surface state resonance [see Fig. 3(d), left], which is reflected in the stronger retardation of VB photoemission calculated and observed at photon energies around 124 eV compared to 145 eV [see Fig. 2(c)].

In conclusion, we find that both the observed resonant enhancement and the attosecond retardation of photoemission are directly linked to the spatial structure of the delocalized sp -band states, necessitating the inclusion of sufficiently complex model potentials and treatment of the electronic structure even in the case of simple metals. By exploiting the synergies between the complementary information obtained from conventional high-resolution photoemission and attosecond streaking we can circumvent the ambiguities that plague relative photoemission time delays without implementation of technically challenging time-zero references [5,20]. Hence, our approach widens the time-domain window into conventional photoemission establishing a connection between energy-space properties of electronic states in solids and the temporal dynamics of the fundamental electronic excitations underlying photoemission spectroscopy. Because of the periodicity of the resonant enhancement and the observed agreement for both the narrow and wide angle of photoemission, our description of the link between the electronic structure of the bound states and the attosecond dynamics of the photoemission process can also be extended to sp -band photoemission deep into the soft-x-ray regime.

We thank F. Siegrist for experimental assistance, and we acknowledge financial support by the Munich Centre for

Advanced Photonics (MAP). R. K. acknowledges an ERC Consolidator Grant “AEDMOS” (ERC-2014-CoG AEDMOS). D.P. acknowledges support from the “MEDEA” (H2020- MSCA-ITN-2014-641789-MEDEA). We thank the Helmholtz-Zentrum Berlin for traveling grants, and the staff of BESSY-II for help during the synchrotron-based experiments. We acknowledge generous infrastructural support from F. Krausz.

*To whom correspondence should be addressed.

johann.riemensberger@tum.de

Present address: École Polytechnique Fédérale de Lausanne (EPFL), Laboratory of Photonics and Quantum Measurements (LPQM), Lausanne CH-1015, Switzerland.

†Present address: Helmholtz-Zentrum Berlin für Materialien und Energie GmbH, 12489 Berlin, Germany.

‡Present address: Ultrafast Innovations GmbH, Am Coulombwall 1, 85748 Garching, Germany.

- [1] A. Damascelli, *Phys. Scr.* **T109**, 61 (2004).
- [2] R. Kienberger, E. Goulielmakis, M. Uiberacker, A. Baltuška, V. Yakovlev, F. Bammer, A. Scrinzi, T. Westerwalbesloh, U. Kleineberg, U. Heinzmann *et al.*, *Nature (London)* **427**, 817 (2004).
- [3] A. L. Cavalieri, N. Müller, T. Uphues, V. S. Yakovlev, A. Baltuška, B. Horvath, B. Schmidt, L. Blümel, R. Holzwarth, S. Hendel *et al.*, *Nature (London)* **449**, 1029 (2007).
- [4] M. Schultze, M. Fieß, N. Karpowicz, J. Gagnon, M. Korbman, M. Hofstetter, S. Neppl, A. L. Cavalieri, Y. Komninos, T. Mercouris *et al.*, *Science* **328**, 1658 (2010).
- [5] M. Ossiander, J. Riemensberger, S. Neppl, M. Mittermair, M. Schäffer, A. Duensing, M. S. Wagner, R. Heider, M. Wurzer, M. Gerl *et al.*, *Nature (London)* **561**, 374 (2018).
- [6] R. Pazourek, S. Nagele, and J. Burgdörfer, *Rev. Mod. Phys.* **87**, 765 (2015).
- [7] M. Ossiander, F. Siegrist, V. Shirvanyan, R. Pazourek, A. Sommer, T. Latka, A. Guggenmos, S. Nagele, J. Feist, J. Burgdörfer *et al.*, *Nat. Phys.* **13**, 280 (2017).
- [8] A. K. Kazansky and P. M. Echenique, *Phys. Rev. Lett.* **102**, 177401 (2009).
- [9] C.-H. Zhang and U. Thumm, *Phys. Rev. Lett.* **102**, 123601 (2009).
- [10] A. G. Borisov, D. Sánchez-Portal, A. K. Kazansky, and P. M. Echenique, *Phys. Rev. B* **87**, 121110 (2013).
- [11] Q. Liao and U. Thumm, *Phys. Rev. Lett.* **112**, 023602 (2014).
- [12] J. C. Baggesen and L. B. Madsen, *Phys. Rev. A* **78**, 032903 (2008).
- [13] C. Lemell, B. Solleder, K. Tkési, and J. Burgdörfer, *Phys. Rev. A* **79**, 062901 (2009).
- [14] S. Neppl, R. Ernstorfer, A. L. Cavalieri, C. Lemell, G. Wachter, E. Magerl, E. M. Bothschafter, M. Jobst, M. Hofstetter, U. Kleineberg *et al.*, *Nature (London)* **517**, 342 (2015).
- [15] M. Lucchini, L. Castiglioni, L. Kasmi, P. Kliuiev, A. Ludwig, M. Greif, J. Osterwalder, M. Hengsberger, L. Gallmann, and U. Keller, *Phys. Rev. Lett.* **115**, 137401 (2015).

- [16] F. Siek, S. Neb, P. Bartz, M. Hensen, C. Strüber, S. Fiechter, M. Torrent-Sucarrat, V. M. Silkin, E. E. Krasovskii, N. M. Kabachnik *et al.*, *Science* **357**, 1274 (2017).
- [17] Z. Tao, C. Chen, T. Szilvasi, M. Keller, M. Mavrikakis, H. C. Kapteyn, and M. M. Murnane, *Science* **353**, 62 (2016).
- [18] F. Roth, T. Arion, H. Kaser, A. Gottwald, and W. Eberhardt, *J. Electron Spectrosc. Relat. Phenom.* **224**, 84 (2018).
- [19] C. Chen, Z. Tao, A. Carr, P. Matyba, T. Szilvási, S. Emmerich, M. Piecuch, M. Keller, D. Zusin, S. Eich *et al.*, *Proc. Natl. Acad. Sci. U.S.A.* **114**, E5300 (2017).
- [20] L. Kasmi, M. Lucchini, L. Castiglioni, P. Kliuiev, J. Osterwalder, M. Hengsberger, L. Gallmann, P. Krüger, and U. Keller, *Optica* **4**, 1492 (2017).
- [21] R. A. Bartynski, R. H. Gaylord, T. Gustafsson, and E. W. Plummer, *Phys. Rev. B* **33**, 3644 (1986).
- [22] S. G. Louie, P. Thiry, R. Pinchaux, Y. Pétrouff, D. Chandesris, and J. Lecante, *Phys. Rev. Lett.* **44**, 549 (1980).
- [23] P. Hofmann, C. Søndergaard, S. Agergaard, S. V. Hoffmann, J. E. Gayone, G. Zampieri, S. Lizzit, and A. Baraldi, *Phys. Rev. B* **66**, 245422 (2002).
- [24] F. Schiller, M. Heber, V. D. P. Servedio, and C. Laubschat, *Phys. Rev. B* **70**, 125106 (2004).
- [25] E. Magerl, S. Neopl, A. L. Cavalieri, E. M. Bothschafter, M. Stanislowski, T. Uphues, M. Hofstetter, U. Kleineberg, J. V. Barth, D. Menzel *et al.*, *Rev. Sci. Instrum.* **82**, 063104 (2011).
- [26] A. Guggenmos, M. Jobst, M. Ossiander, S. Radünz, J. Riemensberger, M. Schäffer, A. Akil, C. Jakubeit, P. Böhm, S. Noever *et al.*, *Opt. Lett.* **40**, 2846 (2015).
- [27] D. A. Shirley, *Phys. Rev. B* **5**, 4709 (1972).
- [28] S. Neopl, R. Ernstorfer, E. M. Bothschafter, A. L. Cavalieri, D. Menzel, J. V. Barth, F. Krausz, R. Kienberger, and P. Feulner, *Phys. Rev. Lett.* **109**, 087401 (2012).
- [29] See Supplemental Material at <http://link.aps.org/supplemental/10.1103/PhysRevLett.123.176801> for further details on the experiments, data analysis and the numerical model, which includes Refs. [30–36].
- [30] D. Spangenberg, E. Rohwer, M. H. Brüggemann, and T. Feurer, *Opt. Lett.* **40**, 1002 (2015).
- [31] M. Lucchini, M. Brüggemann, A. Ludwig, L. Gallmann, U. Keller, and T. Feurer, *Opt. Express* **23**, 29502 (2015).
- [32] V. S. Yakovlev, J. Gagnon, N. Karpowicz, and F. Krausz, *Phys. Rev. Lett.* **105**, 073001 (2010).
- [33] M. Sabbar, S. Heuser, R. Boge, M. Lucchini, T. Carette, E. Lindroth, L. Gallmann, C. Cirelli, and U. Keller, *Phys. Rev. Lett.* **115**, 133001 (2015).
- [34] C. Lemell, S. Neopl, G. Wachter, K. Tkési, R. Ernstorfer, P. Feulner, R. Kienberger, and J. Burgdörfer, *Phys. Rev. B* **91**, 241101 (2015).
- [35] S. Tanuma, C. J. Powell, and D. R. Penn, *Surf. Interface Anal.* **43**, 689 (2011).
- [36] C. Leforestier, R. Bisseling, C. Cerjan, M. Feit, R. Friesner, A. Guldberg, A. Hammerich, G. Jolicard, W. Karrlein, H.-D. Meyer *et al.*, *J. Comput. Phys.* **94**, 59 (1991).
- [37] E. V. Chulkov, V. M. Silkin, and P. M. Echenique, *Surf. Sci.* **437**, 330 (1999).
- [38] S. Neopl, Ph.D. thesis, Technische Universität München, 2012.
- [39] E. E. Krasovskii, W. Schattke, P. Jířek, M. Vondráček, O. V. Krasovska, V. N. Antonov, A. P. Shpak, and I. Bartoš, *Phys. Rev. B* **78**, 165406 (2008).